Functional heterogeneity of cytotoxic T cells and tumor resistance to cytotoxic hits limit anti-tumor activity in vivo

Roxana Khazen, Marine Cazaux, Fabrice Lemaître, Beatrice Corre, Zacarias Garcia, Philippe Bousso

Revised

CTL functional heterogeneity and tumor resistance to cytotoxic hits limit anti-tumor activity *in vivo*

Roxana Khazen[1], Marine Cazaux[1,2], Fabrice Lemaître[1], Beatrice Corre[1], Zacarias Garcia[1] and Philippe Bousso[1]

[1] Dynamics of Immune Responses Unit, Institut Pasteur, Equipe Labellisée Ligue Contre le Cancer, INSERM U1223, 75015 Paris, France.

[2] University Paris Diderot, Sorbonne Paris Cité, 75015 Paris, France.

Correspondence to philippe.bousso@pasteur.fr

Abstract

Cytotoxic T cells can eliminate tumor cells through the delivery of lethal hits but the actual efficiency of this process in the tumor microenvironment is unclear. Here we visualized the capacity of single CTLs to attack tumor cells *in vitro* and *in vivo* using genetically-encoded reporters to monitor cell damage and apoptosis. Using two distinct tumor B cell lines, we found that, despite proper immunological synapse formation, the majority of cytotoxic hits delivered by CTLs *in vitro* were sublethal, associated with reversible calcium elevation and membrane damage in the targets. Using intravital imaging in the bone marrow, we established that the majority of CTL interactions with lymphoma B cells were either unproductive or sublethal. This diversity of tumor cell fate was partly accounted for by functional CTL heterogeneity. In the therapeutic settings of anti-CD19 CAR T cells also, the majority of CAR T cell-tumor interactions were not associated with lethal hit delivery. Thus, differences in CTL lytic potential together with tumor cell resistance to cytotoxic hits represent two important bottlenecks for anti-tumor responses *in vivo*.

Synopsis and bullet points

The efficiency of CTL or CAR T cell lethal hit delivery in the tumor microenvironment is unclear. Here, intravital imaging and functional reporters were used to quantify the various outcomes of T cell-tumor contacts, revealing that a minority of interactions resulted in target cell killing.

• Most CTL-tumor cell contacts are non-lethal

• Tumor cells often recover from CTL-induced membrane damage

• CTLs or CAR T cells exhibit extensive variability in killing capacities in vivo

Keywords: CTL, CAR T cells, lethal hit, sublethal hit, intravital imaging

Introduction

Cytotoxic T cells (CTLs) have the ability to kill infected and tumor cells. Upon CTL conjugation with cognate target cells, CTLs release perforin and granzymes to form pores in the plasma membrane and initiate cell death, respectively. The molecular and cellular dynamics of CTL-mediated killing have been studied extensively *in vitro* (Basu & Huse, 2017; Dieckmann *et al*, 2016; Dustin & Long, 2010). These studies revealed in particular that CTL killing is a highly sensitive and rapid process (Bertrand *et al*, 2013; Wiedemann *et al*, 2006). Moreover, when CTL activity in culture was analyzed at the single cell level, extensive heterogeneity in CTL killing performance was recorded with a fraction of CTLs endowed with the ability to kill multiple targets (Varadarajan *et al*, 2011; Vasconcelos *et al*, 2015). These studies also highlighted that cytotoxic effectors such as NK cells or T cells can increase their killing abilities over time, exhibiting burst killing behaviors (Choi & Mitchison, 2013; Vasconcelos *et al.*, 2015). In the context of cancer, another layer of complexity comes from the fact that tumor cells often exhibit resistance to cell death and reduced sensitivity to granzymes (Kashkar *et al*, 2006; Lickliter *et al*, 2007; Mohammad *et al*, 2015). Beyond the down regulation of antigen presentation, tumors may also exhibit specific mechanisms to resist CTL-mediated cytotoxic hits (Khazen *et al*, 2016; Medema *et al*, 2001). Melanoma cells for instance can use lysosome secretion at the immunological synapse to counteract perforin activity (Khazen *et al.*, 2016).

While these *in vitro* studies have been instrumental to delineate key features of CTL biology, it remains unclear how efficiently CTL exert their cytolytic function in the microenvironment (TME) of a developing tumor. A few studies have relied on intravital imaging as a mean to monitor CTL killing activity at the single cell level in different contexts. In a model of solid tumor, the average killing frequency per CTL was one every 6 hours (Breart *et al*, 2008). CTL

delivery of lethal hits to B cell targets in lymph nodes was found to be largely suppressed by regulatory T cells (Mempel *et al*, 2006). In the context of CAR T cells, we recently reported extensive heterogeneity in CAR T cell signaling upon target encounter and subsequent cytotoxic activity (Cazaux *et al*, 2019). Finally, in a model of viral infection, CTL killing was only efficient when multiple T cells were collectively hitting the target cell (Halle *et al*, 2016). Together, these studies have indicated that CTL-mediated killing may not be a very efficient process *in vivo*. Suboptimal CTL activity may arise from the inability to recognize tumor targets, failure to deliver cytotoxic hits, or lack of target cell death despite the delivery of cytotoxic cargo. Understanding the outcomes of individual CTL-tumor cell interactions *in vivo* is therefore essential to obtain a comprehensive picture of intratumoral CTL activity.

Here, we have used a combination of fluorescent reporters to track target cell damage and induction of apoptosis during CTL activity against a B cell lymphoma. We report that most CTL-tumor cell contacts are either unproductive or induce sublethal damages and that only a minority of interactions results in tumor cell killing. Furthermore, we provide evidence that individual CTLs exhibit heterogeneous behavior and lytic activities *in situ*. Our results suggest that suboptimal T cell cytotoxic activity and tumor resistance to lethal hits represent important bottlenecks for tumor elimination.

Results

Diverse outcomes for tumor cells in response to CTL attack

To quantify the efficiency of CTL-mediated killing, we relied on OT-I T cells and a Myc-driven B cell lymphoma tumor cell line expressing the ovalbumin (OVA) model antigen. We examined CTL activity in a classic *in vitro* cytotoxic assay performed in a U-bottom plate. Tumor killing was very efficient in these settings even at low E:T ratio (2:1) with 65% of targets eliminated within 4h (**Figure 1A**). This result confirmed that OVA-expressing B lymphoma cells are sensitive to CTL killing. Of note, tumor cell elimination by CTLs significantly dropped when the cytotoxic assay was performed in a flat-bottom plate at the same E:T ratio (**Figure 1A**). The perforin/granzyme pathway was likely dominant at least in the time frame of the assay as killing was largely abolished by calcium chelation (that blocks granule exocytosis) **(Appendix Figure S1A**). Since we cannot formally exclude that calcium chelation affects other pathways, we also analyzed granzyme B activity within targets cells loaded with a specific substrate. As shown in **Appendix Figure S1B and S1C**, we rapidly detected granzyme B activity within tumors cells cocultured with CTLs. The lower efficiency of CTL killing in flat-bottom plate may reflect the fact that not all target cells were in contact with a CTL during the assay. It is also possible that most CTL were efficiently paired to tumor cells but that a minority of contacts triggered cell death. To test the latter possibility, we imaged CTL-tumor cell conjugates with the aim to visualize both target cell damage and induction of apoptosis. Pore-formation during delivery of cytotoxic hit has been associated with entry of extracellular calcium (and therefore an increase in intracellular calcium concentration) and of other small molecules present in the extracellular milieu (including propidium iodide (PI)) (**Figure 1B**) (Keefe *et al*, 2005; Lopez *et al*, 2013; Poenie *et al*, 1987).

We first labeled CTLs and tumor cells with the calcium sensitive dye Indo-1 and added PI in the culture. As expected, CTLs exhibited a calcium signal upon conjugation with the target cells, indicative of effective antigenic recognition (**Figure 1C-D, Movie 1**). In 54% (87/161) of the conjugates, this was followed by an elevation of intracellular calcium concentration in the target cell (**Figure 1C-D, Movie EV1**). In most of these conjugates, calcium elevation was concomitant with a progressive entry of PI in the target cell, suggesting that membrane damage (induced by perforin-pore formation) was responsible for calcium entry (**Figure 1C-D, Movie EV1**). Two outcomes were then recorded. Target cell death (corresponding to lethal hits) as reflected by bright PI staining and persistent calcium elevation was detected in less than 20% of conjugates with membrane damage (**Figure 1C-D, Movie EV1**). The remaining target cells appeared to survive the attack (sublethal hit) with intracellular calcium returning to baseline levels and no further PI uptake being detected (**Figure 1C-D, Movie 1**). This was most likely due to the existence of repair mechanisms that help restore membrane integrity after perforin pore formation (Keefe *et al.*, 2005; Khazen *et al.*, 2016; Lopez *et al.*, 2013). Finally, in approximately half of the conjugates (46%), we did not detect evidence for membrane damage (no hits: no calcium elevation nor PI uptake in the target), despite the fact that all CTLs exhibited potent calcium elevation upon target cell conjugation (**Figure 1C-D, Movie EV1**). Overall, as summarized in **Figure 1E**, diverse tumor cell fates were observed following conjugate with a CTL. Moreover, in a different B cell lymphoma model (pro B cells driven by v-Abl expression (Lenden Hasse *et al*, 2017), we again observed that the majority of CTLs contacts did not lead to lethal hit delivery (**Figure 1E**) indicating that sublethal hits are not restricted to Myc-driven B cell lymphomas.

A minority of CTL-tumor cell interactions results in target cell apoptosis *in vitro*

To directly monitor the induction of apoptosis in target cells in conjunction with calcium signals, we used B cell tumors expressing a genetically-encoded caspase 3 reporter (Cazaux *et al.*, 2019) and labeled these cells with Indo-1. We found that a majority of tumor cells paired with a CTL exhibited one or several calcium fluxes, while calcium fluxes were much less frequent and shorter in duration in isolated tumors (**Figure 2A-D**).

Distinct outcomes were observed for CTL-tumor cell conjugates (**Figure 2E-F, Movie EV2**). Calcium elevation in target cells was most often transient and not associated with apoptosis induction. These results were consistent with the delivery of sublethal hits inducing pore formation but rapid repair. As shown in **Figure 2E-F** and **Movie EV2**, only a minority of CTL-target pairs (7%) displayed evidence of cell damage (calcium flux) followed by apoptosis induction (lethal hits).

Killing events were associated with longer calcium increases (>12 min) while calcium elevation rarely exceeds 5 min in sublethal responses suggesting that sustained calcium elevation could be used as a proxy to target killing (**Figure 1D**, **Figure 2B, F**).
In sum, the study of stable CTL-tumor cell conjugates strongly suggests that despite effective target cell recognition, CTL often fail to trigger a lethal response in tumor targets, inducing instead either no detectable effects or a sublethal response.

Stable immunological synapse formation between CTLs and tumor cells does not predict target cell fate

It was possible that the quality of the immunological synapse formed between the CTL and the target cell dictated the efficacy of the killing process. We therefore compared the characteristics of CTL-tumor conjugates for interactions associated with no, sublethal or

lethal hits. We used LifeAct-GFP-expressing CTLs (to monitor actin accumulation) and the genetically-encoded Twitch-2B calcium indicator (to assess target cell responses to CTL attack). One hallmark of conjugate formation is the rounding of CTLs (Donnadieu *et al*, 1994; Negulescu *et al*, 1996). As shown in **Figure 3A-D**, CTL rounding was similar for T cells triggering no, sublethal or lethal hits. We also quantified actin accumulation at the CTL-tumor cell interface. Robust actin accumulation was detected in all conjugates, irrespective of the final tumor cell fate (**Figure 3C, E**). These results suggest that the low rate of successful killing by CTLs when analyzed at the single cell level is not the consequence of defective synapse formation.

Intratumoral CTL activity is dominated by the delivery of sublethal hits

Having established the diversity of tumor cell fates following CTL conjugation *in vitro*, we sought to quantify the outcome of CTL attack at the single cell level *in vivo*. For this, we used mice with established B cell lymphoma expressing the OVA antigen and the Twich2B genetically-encoded calcium reporter. As reported previously, bone marrow was the primary site of tumor development (Cazaux *et al.*, 2019). Activated OT-I $CD8^+$ T cells were transferred as a model of adoptive T cell therapy, and intravital imaging was performed 2 days later. We examined the response of individual tumor cells during their interactions with CTLs in comparison to tumors developing in the absence of T cells. Consistent with our *in vitro* data, calcium fluxes were largely increased (both in duration and numbers) in tumor cells contacted by CTLs, indicating that a substantial fraction of tumor cells are responding to CTL attack (**Figure 4A-E, Appendix Figure S2A, Movie EV3**). However, most of these calcium rises were transient, suggestive of sublethal interactions (**Figure 4B, Movie EV3**). A minority of contact resulted in prolonged calcium elevation in tumor cells, an observation compatible with irreversible membrane damage (**Figure 4B**). Although killing could not be

directly ascertained in these experiments, our measurements of prolonged calcium responses indicated that, at most, 6 % of the CTL-tumor contacts were lethal (**Figure 4B, F**). In sum, our single-cell imaging of CTL activity *in vivo* suggested that tumor cells most often survive individual CTL attack, a feature that most likely limits the efficacy of anti-tumor T cell responses.

CTL functional heterogeneity during interactions with tumor cells *in vivo*

In addition to potential heterogeneity within tumor cells, it is possible that not all CTLs exhibited the same capacity of hit delivery at the time of imaging. To test this possibility, we tracked individual CTLs for 2-4 h and analyzed the outcome of all their interactions with tumor cells. First, we examined calcium responses elicited in all target cells contacted by individual CTLs. As illustrated in **Figure 5A-B**, extensive differences were observed in the calcium responses elicited by distinct CTLs. Some CTLs induced no or little calcium elevation in the contacted targets, while other efficiently triggered a calcium response in the majority of contacted targets. Second, we imaged apoptosis induction in tumor cells contacted by individual CTLs *in vivo*, using B lymphoma cells expressing the FRET-based reporter for caspase 3 activity. Extensive heterogeneity in killing efficiency was apparent in these experiments, with some T cells killing rapidly and successfully multiple targets, while others failed to kill any tumor cells over multiple hours (**Figure 5C-E** and **Movie EV4-5**). These observations likely represent *in vivo* evidence for the previous *in vitro* description of super-killer cells within the CTL pool (Vasconcelos *et al.*, 2015). Only 20% of CTLs were capable of inducing tumor cell death during the imaging period, and killing events represented 5% of all total contacts established (**Figure 5C-E**). Taken together, our results suggest that functional heterogeneity in CTLs contributes to the diverse outcomes during CTL-tumor contacts *in vivo*.

A minority of interactions established by CAR T cells lead to lethal hit delivery

To extend our findings to a therapeutic setting, we analyzed the tumor cell fate upon contact with anti-CD19 CAR T cells. As observed with CTLs, CAR T cells triggered calcium elevation in target cells (**Figure 6A-D, Movie EV6**). Although tumor killing by CAR T cells was more efficient than by conventional CTLs (compared Figure 2 and Figure 6), still in most cases, calcium signals in tumors were reversible, suggesting frequent delivery of sublethal hit by CAR T cells (**Figure 6E, Movie EV6**). Next, we examined CAR T cell interaction with B cell tumors *in vivo* by intravital imaging. CAR T cells increased the frequency of calcium responses in contacted targets as compared to non contacted targets in the same region or tumors without CAR T cell transfer (**Figure 7A-D**, **Appendix Figure S2B**). However, only a small percentage of contacted targets (10%) exhibited a prolonged calcium response compatible with a lethal hit delivery (**Figure 7E, Movie EV7**). Functional heterogeneity in CAR T cells contributed to the diversity of contact outcome as some CAR T cells induced calcium responses in multiple contacted targets while others were seen interacting extensively with tumors eliciting little or no detectable response (**Figure 7F-G**). Thus, the outcome of CAR T cell interactions with tumors appears highly diverse with only a fraction of contacts leading to lethal hit delivery.

Discussion

By means of intravital imaging and functional reporters in tumor cells, we have established here that, despite effective antigen recognition, intratumoral CTLs and CAR T cells often fail to deliver lethal hits. Overall, less than 10% of CTL-tumor cell contacts resulted in tumor cell killing. The large majority of CTL-tumor cell contact appeared to induce reversible damage or no detectable damage at all.

Our results extend findings by Halle et al. that have observed low killing rate and sublethal interactions in the context of virally infected cells in lymph node (Halle *et al.*, 2016). One notable difference with the viral infection model in which killing occurred during swarming of multiple T cells around the target is that the CTLs density within the TME was found to be lower, limiting CTL cooperativity. Here and in previous tumor imaging studies (Breart *et al.*, 2008; Cazaux *et al.*, 2019), tumor killing (although unfrequent) was most often the result of a monogamous interaction. Virus and tumors may also have both shared and unique mechanisms for suppressing CTL activity. In particular, several mechanisms could concur to the surprisingly low rate of intratumoral CTL- or CAR T cell-mediated killing when this phenomenon was analyzed at the single cell level. Dampening of T cell responsiveness in the TME, the presence of regulatory T cells and functional exhaustion may decrease the ability of CTL to arrest on their target and degranulate (Boldajipour *et al*, 2016; Mempel *et al.*, 2006; Michonneau *et al*, 2016). Additionally, tumor cells can develop mechanisms to resist cytotoxic hits and rapidly repair membrane damages (Khazen *et al.*, 2016; Lopez *et al.*, 2013; Medema *et al.*, 2001). Consistently, we provide evidence for frequent delivery of sublethal hits in the TME. Our result implies that a high density of CTLs is most likely required for

tumor regression, in order to increase the probability of killing (Beck *et al*, 2020; Deguine & Bousso, 2013; Halle *et al.*, 2016; Hamieh *et al*, 2019). This has been indeed predicted by modeling approach (Budhu *et al*, 2010) and consistently, we had previously observed in two distinct models that tumor regression was associated with the progressive accumulation of cytotoxic effectors (Breart *et al.*, 2008; Cazaux *et al.*, 2019). In addition, our present finding that only a fraction of CTLs exhibit strong cytotoxic potential at a given time point also suggests that functional heterogeneity in CTLs represents an important bottleneck in tumor eradication. Previous *in vitro* studies have indicated that not all CTLs are equally efficient at killing cognate targets (Snyder *et al*, 2003; Vasconcelos *et al.*, 2015) and it is possible that this heterogeneity is further increased by stochastic events *in vivo* such as CTL history of previous cellular encounters. It is important to note that in addition to CTLs, tumor cells present in a given individual can also exhibit extensive heterogeneity (Marusyk *et al*, 2012; Milo *et al*, 2018), further contributing to the diversity of outcomes during CTL-tumor contacts.

One limitation of the study is that assessment of target killing and tumor damage was performed during and immediately after CTLs contacts. This is due in part to the technical difficulty to image individual tumors for extended periods *in vivo*. While calcium signals in target cells have been largely attributed to the perforin/granzyme pathway (Halle *et al.*, 2016), it remains theoretically possible that distinct types of cell death are induced at later time points. The generation of genetically-encoded reporter for other cell death pathways may help clarify the relative contribution of caspase 3-independent cell death pathways in tumor regression.

As illustrated here, the ability to measure the consequence of single CTL-tumor cell interactions should provide a framework to evaluate strategies aimed at boosting lethal hit delivery by a maximal number of tumor-infiltrating T cells.

Materials and Methods

Mice and cell lines

Six to eigth week-old C57BL/6J mice were purchased from Charles River and ENVIGO. *Rag1*$^{-/-}$ LifeAct-GFP OT-I TCR or Ubi-GFP *Rag1*$^{-/-}$ OT-I TCR, Eμ-myc, and *Rag2*$^{-/-}$ mice were bred in our animal facility under specific pathogen–free conditions. All animal studies were approved by the Institut Pasteur Safety Committee in accordance with French and European guidelines (CETEA 2017-0038).

A lymphoma B cell line was isolated from a male Eμ-myc transgenic mouse (Harris *et al*, 1988), which develops spontaneous Burkitt-like B cell lymphomas. Immortalized pro-B cells were generated by infecting bone marrow cells with retro virus encoding for viral-Abelson kinase (v-abl) (Lenden Hasse *et al.*, 2017). Both cell lines were retrovirally transduced to express OVA antigen and Eμ-myc cells were additionally transduced to express either the FRET-based Twitch-2B calcium indicator (Eμ-myc-Twitch-2B) (Thestrup *et al*, 2014) or a FRET-based reporter for caspase-3 activity (Eμ-myc-DEVD) (Cazaux *et al.*, 2019). Cells were cultured in complete RPMI medium and were routinely tested for the absence of Mycoplasma contamination (Venor-GeM Advance mycoplasma detection kit, Minerva Biolabs).

In vitro cytotoxicity assay

Target cells were washed and subsequently transferred to a 96-well U-bottom or flat bottom plate at 10^5 in 100 µl of complete RPMI. Activated OTI-GFP T cells were added to the target cells at an effector:target ratio of 2:1. Cells were pelleted for 1 min and incubated at 37 °C for the indicated periods. The number of live cells was counted on a Cytoflex LX (Beckman Coulter).

In vitro imaging of CTL-tumor cell interactions

Plastic dishes were coated with Poly-D-Lysine (Sigma, 0.01% dilution in H_2O) for 10 min at 37°C and then with 5 µg/mL recombinant mouse ICAM-1 (R&D systems) for 1 h at 37 °C. Targets and/or T cells were stained with Indo-1/AM (2.5 µM, Molecular Probes) for 40 min at 37 °C. Cells were then washed and transferred in plastic dishes in complete RPMI without phenol red and when indicated 100 µM propidium iodide (Sigma) was added at the beginning of image acquisition. *In vitro* imaging was performed using a two-photon microscope. Excitation was provided by an Insight DS+ Dual laser (Spectra-Physics) tuned at either 720, 880 or 1040 nm. The following filter sets were used for imaging Indo-1 and propidium iodide (Indo-1: 483/32 and 390/40, and PI: 624/40), Twitch-2B and DEVD (CFP: 483/32 and YFP: 542/27). Ca^{2+} signals were quantified using the ratio of calcium bound to calcium free fluorescence (Indo-1, 720nm excitation) or using the ratio of YFP to CFP fluorescence (Twitch-2B, 880 nm excitation) as described (Bohineust *et al*, 2020). PI uptake was measured by evaluating PI fluorescence in target cells over time. Images were analyzed using Fiji software.

Generation of CTLs and CAR T cells

Splenocytes were isolated from *Rag1*$^{-/-}$ LifeAct-GFP OT-I TCR or Ubi-GFP OT-I TCR transgenic mice and red blood cells were removed by ammonium–chloride–potassium lysis. One-third of the cells was then pulsed with 50 µM of $OVA^{257–264}$ peptide (SIINFEKL) for 2 h at 37 °C. The rest of the cells was incubated at 37 °C in complete medium. The two populations were mixed and cultured for 3 days. Cells were then subjected to Ficoll gradient centrifugation to remove dead cells, and cultured in complete medium containing human IL-2 (210 IU/ml; R&D) for 4 additional days. Anti-CD19 CAR T cells were generated as described previously (Cazaux *et al.*, 2019) using lymph nodes from *Rag1*$^{-/-}$ Ubi-GFP OT-I TCR

transgenic mice. T cells were activated in plates pre-loaded with 2.5 µg anti-CD3 mAb (clone 17.A2; BioLegend) and of 2.5 µg/ml soluble anti-CD28 mAb (clone 37.51; BioLegend) with 10 ng/ml murine IL-12 (Andrikauskatie 2015; SRP3204; Sigma-Aldrich). T cells were transduced using the tCD34.2A.amCD19.CD28IEVζ retroviral vector (Cazaux *et al.*, 2019). CAR T cells were cultured for 4 additional days in the presence of of hIL-2.

Tumor establishment and adoptive T cell transfer

B cell lymphomas (Eµ-myc-Twitch-2B or Eµ-myc-DEVD lines) were established by i.v injection of 0.5 × 10^6 cells in $Rag2^{-/-}$ mice or in C57BL/6 mice conditioned by a sublethal irradiation (4 Gy). T cells or CAR T cells (10-20x10^6) were injected i.v. on the indicated day.

Intravital imaging

Bone marrow intravital imaging was performed 40 h after T cell transfer as previously described (Cazaux *et al.*, 2019). Two-photon imaging was performed with an upright microscope FVMPE-RS (OLYMPUS) and a 25×/1.05 NA water-dipping objective (OLYMPUS). Excitation was provided by an Insight deep see dual laser (Spectra Physics) tuned at 880 nm. A 25-µm-thick volume of tissue was scanned at 5-µm Z-steps and 30 to 40 s intervals. Images were processed and analyzed using Fiji software. Videos and figures based on two-photon microscopy are shown as two-dimensional maximum intensity projections of three-dimensional data.

Statistical analysis

All statistical tests were performed with Prism v.6.0b (GraphPad). Unpaired t-tests were used as indicated.

Data Availability

This study includes no data deposited in external repositories

Acknowledgements

We thank members of the Bousso laboratory for critical review of the manuscript. We thank the mouse facility and Technology Core of the Center for Translational Science (CRT) at Institut Pasteur for support in conducting the present study. The work was supported by Institut Pasteur, INSERM and an advanced grant (ENLIGHTEN) from the European Research Council. R.K. was supported by fellowships from the Canceropole and Fondation ARC.

Author contributions

R.K., M.C. B.C., Z.G. and F.L conducted the experiments. R.K., M.C. and P.B. designed the experiments. R.K. and P.B. analyzed the data and wrote the manuscript.

Conflict of Interest

The authors declare no conflict of interests.

References

Basu R, Huse M (2017) Mechanical Communication at the Immunological Synapse. *Trends Cell Biol* 27: 241-254

Beck RJ, Bijker DI, Beltman JB (2020) Heterogeneous, delayed-onset killing by multiple-hitting T cells: Stochastic simulations to assess methods for analysis of imaging data. *PLoS Comput Biol* 16: e1007972

Bertrand F, Muller S, Roh KH, Laurent C, Dupre L, Valitutti S (2013) An initial and rapid step of lytic granule secretion precedes microtubule organizing center polarization at the cytotoxic T lymphocyte/target cell synapse. *Proc Natl Acad Sci U S A* 110: 6073-6078

Bohineust A, Garcia Z, Corre B, Lemaitre F, Bousso P (2020) Optogenetic manipulation of calcium signals in single T cells in vivo. *Nat Commun* 11: 1143

Boldajipour B, Nelson A, Krummel MF (2016) Tumor-infiltrating lymphocytes are dynamically desensitized to antigen but are maintained by homeostatic cytokine. *JCI Insight* 1: e89289

Breart B, Lemaitre F, Celli S, Bousso P (2008) Two-photon imaging of intratumoral CD8 T cell cytotoxic activity during adoptive T cell therapy in mice. *J Clin Invest* 118: 1390-1397

Budhu S, Loike JD, Pandolfi A, Han S, Catalano G, Constantinescu A, Clynes R, Silverstein SC (2010) CD8(+) T cell concentration determines their efficiency in killing cognate antigen expressing syngeneic mammalian cells in vitro and in mouse tissues. *Journal of Experimental Medicine* 207: 223-235

Cazaux M, Grandjean CL, Lemaitre F, Garcia Z, Beck RJ, Milo I, Postat J, Beltman JB, Cheadle EJ, Bousso P (2019) Single-cell imaging of CAR T cell activity in vivo reveals extensive functional and anatomical heterogeneity. *J Exp Med*

Choi PJ, Mitchison TJ (2013) Imaging burst kinetics and spatial coordination during serial killing by single natural killer cells. *Proc Natl Acad Sci U S A* 110: 6488-6493

Deguine J, Bousso P (2013) Dynamics of NK cell interactions in vivo. *Immunol Rev* 251: 154-159

Dieckmann NM, Frazer GL, Asano Y, Stinchcombe JC, Griffiths GM (2016) The cytotoxic T lymphocyte immune synapse at a glance. *J Cell Sci* 129: 2881-2886

Donnadieu E, Bismuth G, Trautmann A (1994) Antigen recognition by helper T cells elicits a sequence of distinct changes of their shape and intracellular calcium. *Curr Biol* 4: 584-595

Dustin ML, Long EO (2010) Cytotoxic immunological synapses. *Immunol Rev* 235: 24-34

Halle S, Keyser KA, Stahl FR, Busche A, Marquardt A, Zheng X, Galla M, Heissmeyer V, Heller K, Boelter J *et al* (2016) In Vivo Killing Capacity of Cytotoxic T Cells Is Limited and Involves Dynamic Interactions and T Cell Cooperativity. *Immunity* 44: 233-245

Hamieh M, Dobrin A, Cabriolu A, van der Stegen SJC, Giavridis T, Mansilla-Soto J, Eyquem J, Zhao Z, Whitlock BM, Miele MM *et al* (2019) CAR T cell trogocytosis and cooperative killing regulate tumour antigen escape. *Nature* 568: 112-116

Harris AW, Pinkert CA, Crawford M, Langdon WY, Brinster RL, Adams JM (1988) The E mu-myc transgenic mouse. A model for high-incidence spontaneous lymphoma and leukemia of early B cells. *The Journal of experimental medicine* 167: 353-371

Kashkar H, Seeger JM, Hombach A, Deggerich A, Yazdanpanah B, Utermohlen O, Heimlich G, Abken H, Kronke M (2006) XIAP targeting sensitizes Hodgkin lymphoma cells for cytolytic T-cell attack. *Blood* 108: 3434-3440

Keefe D, Shi L, Feske S, Massol R, Navarro F, Kirchhausen T, Lieberman J (2005) Perforin triggers a plasma membrane-repair response that facilitates CTL induction of apoptosis. *Immunity* 23: 249-262

Khazen R, Muller S, Gaudenzio N, Espinosa E, Puissegur MP, Valitutti S (2016) Melanoma cell lysosome secretory burst neutralizes the CTL-mediated cytotoxicity at the lytic synapse. *Nat Commun* 7: 10823

Lenden Hasse H, Lescale C, Bianchi JJ, Yu W, Bedora-Faure M, Deriano L (2017) Generation and CRISPR/Cas9 editing of transformed progenitor B cells as a pseudo-physiological system to study DNA repair gene function in V(D)J recombination. *J Immunol Methods* 451: 71-77

Lickliter JD, Cox J, McCarron J, Martinez NR, Schmidt CW, Lin H, Nieda M, Nicol AJ (2007) Small-molecule Bcl-2 inhibitors sensitise tumour cells to immune-mediated destruction. *Br J Cancer* 96: 600-608

Lopez JA, Susanto O, Jenkins MR, Lukoyanova N, Sutton VR, Law RH, Johnston A, Bird CH, Bird PI, Whisstock JC *et al* (2013) Perforin forms transient pores on the target cell plasma membrane to facilitate rapid access of granzymes during killer cell attack. *Blood* 121: 2659-2668

Marusyk A, Almendro V, Polyak K (2012) Intra-tumour heterogeneity: a looking glass for cancer? *Nat Rev Cancer* 12: 323-334

Medema JP, de Jong J, Peltenburg LT, Verdegaal EM, Gorter A, Bres SA, Franken KL, Hahne M, Albar JP, Melief CJ *et al* (2001) Blockade of the granzyme B/perforin pathway through overexpression of the serine protease inhibitor PI-9/SPI-6 constitutes a mechanism for immune escape by tumors. *Proc Natl Acad Sci U S A* 98: 11515-11520

Mempel TR, Pittet MJ, Khazaie K, Weninger W, Weissleder R, von Boehmer H, von Andrian UH (2006) Regulatory T cells reversibly suppress cytotoxic T cell function independent of effector differentiation. *Immunity* 25: 129-141

Michonneau D, Sagoo P, Breart B, Garcia Z, Celli S, Bousso P (2016) The PD-1 Axis Enforces an Anatomical Segregation of CTL Activity that Creates Tumor Niches after Allogeneic Hematopoietic Stem Cell Transplantation. *Immunity* 44: 143-154

Milo I, Bedora-Faure M, Garcia Z, Thibaut R, Perie L, Shakhar G, Deriano L, Bousso P (2018) The immune system profoundly restricts intratumor genetic heterogeneity. *Sci Immunol* 3

Mohammad RM, Muqbil I, Lowe L, Yedjou C, Hsu HY, Lin LT, Siegelin MD, Fimognari C, Kumar NB, Dou QP *et al* (2015) Broad targeting of resistance to apoptosis in cancer. *Semin Cancer Biol* 35 Suppl: S78-S103

Negulescu PA, Krasieva TB, Khan A, Kerschbaum HH, Cahalan MD (1996) Polarity of T cell shape, motility, and sensitivity to antigen. *Immunity* 4: 421-430.

Poenie M, Tsien RY, Schmitt-Verhulst AM (1987) Sequential activation and lethal hit measured by [Ca2+]i in individual cytolytic T cells and targets. *EMBO J* 6: 2223-2232

Snyder JE, Bowers WJ, Livingstone AM, Lee FEH, Federoff HJ, Mosmann TR (2003) Measuring the frequency of mouse and human cytotoxic T cells by the Lysispot assay: independent regulation of cytokine secretion and short-term killing. *Nature Medicine* 9: 231-235

Thestrup T, Litzlbauer J, Bartholomaus I, Mues M, Russo L, Dana H, Kovalchuk Y, Liang Y, Kalamakis G, Laukat Y *et al* (2014) Optimized ratiometric calcium sensors for functional in vivo imaging of neurons and T lymphocytes. *Nat Methods* 11: 175-182

Varadarajan N, Julg B, Yamanaka YJ, Chen H, Ogunniyi AO, McAndrew E, Porter LC, Piechocka-Trocha A, Hill BJ, Douek DC *et al* (2011) A high-throughput single-cell analysis of human CD8(+) T cell functions reveals discordance for cytokine secretion and cytolysis. *J Clin Invest* 121: 4322-4331

Vasconcelos Z, Muller S, Guipouy D, Yu W, Christophe C, Gadat S, Valitutti S, Dupre L (2015) Individual Human Cytotoxic T Lymphocytes Exhibit Intraclonal Heterogeneity during Sustained Killing. *Cell Rep* 11: 1474-1485

Wiedemann A, Depoil D, Faroudi M, Valitutti S (2006) Cytotoxic T lymphocytes kill multiple targets simultaneously via spatiotemporal uncoupling of lytic and stimulatory synapses. *Proc Natl Acad Sci U S A* 103: 10985-10990

Figure legends

Figure 1: Visualizing the various tumor cell fates in response to CTL attack *in vitro*

(**A**) OVA-expressing lymphoma B cells are killed by OT-I CTL in a bulk cytotoxic assay. OT-I CTLs were cultured in the presence of OVA^+ Eμ-myc B cells in either U-bottom (white) or flat-bottom (grey) plates. Tumor cell killing was evaluated by flow cytometry at the indicated time points. Data were pooled from three independent experiments with 3 distinct image acquisitions in each experiment. (***$p<0.001$, unpaired t-test).

(**B**) Scheme illustrating that perforin-mediated pore formation promotes the entry of calcium and propidium iodide (PI) in the cytosol of target cells.

(**C-D**) Diverse outcome for tumor cells following interactions with CTLs. OT-I CTLs and OVA^+ Eμ-myc B cells were labeled with the calcium-sensitive dye Indo-1, cultured together in the presence of propidium iodide (PI) and subjected to live imaging. Representative time-lapse images (**C**) and corresponding fluorescence quantification (**D**) showing the three distinct outcomes for CTL-tumor cell contacts (left, calcium response in T cells, and right, calcium and PI signal in targets): no detectable damage (no calcium signal in the target cells), reversible damage (transient calcium elevation and low uptake of PI), and irreversible damage (prolonged calcium elevation and bright PI staining). CTLs are outlined by white dashed lines. White arrowheads indicate tumor cells. Red arrowheads indicate tumor cells with internalized PI. Scale bar, 5 μm.

(**E**) Pie chart representing the various fates of tumor cells following conjugation with a CTL. Data were pooled from three independent experiments with 3 distinct image acquisitions in each experiment.

Figure 2: A minority of CTL-tumor cell interactions results in target cell apoptosis *in vitro*

OVA^{+}Eμ-myc B cells expressing a FRET-based reporter for caspase 3 activity were labeled with the calcium-sensitive dye Indo-1, incubated with OT-I CTLs and subjected to live imaging.

(**A-B**) Calcium responses were recorded over time in (**A**) unconjugated tumor cells or in (**B**) tumor cells forming a conjugate with a CTL (during the duration of the contacts). Each line corresponds to an individual tumor cell and each square to a time point. Squares are colored in magenta upon calcium elevation or in blue otherwise. Apoptotic events (detected by caspase 3 activity) are indicated by an overlaid green dot. Data is representative of three independent experiment.

(**C**) The number of calcium fluxes in individual tumor cells is plotted for unconjugated tumors or conjugated tumors. Values were normalized to 100 min. Each dot represents one tumor cell. Bars represent mean values.

(**D**) The cumulated period of calcium signals was recorded for individual unconjugated or conjugated target cells and expressed as percentage of total time. Each dot represents one tumor cell. Bars represent mean values.

(**E-F**) Distinct tumor cell outcomes in response to CTL attack. Three categories were defined: no hit (no calcium response in the target cell), sublethal hit (transient calcium response and no caspase 3 activity), lethal hit (prolonged calcium response and induction of caspase 3 activity). (**E**) Pie chart representing the percentage of each category. (**F**) Time-lapse images (left) of a representative CTL-tumor cell conjugate in each of the three categories are shown together with the corresponding quantification (right) of calcium response and caspase 3 activity over time. T cells are delineated by white dashed lines. Scale bar, 10 μm. Data were pooled from three independent experiments. (**$p<0.01$, unpaired t-test).

Figure 3: The formation of the immunological synapse does not predict target outcome during CTL-tumor cell contacts

LifeAct-GFP OT-I CTLs were cultured with B lymphoma cells expressing the OVA model antigen and the genetically-encoded calcium indicator Twich2B.

(**A**) Representative time-lapse image illustrating CTL rounding upon target engagement. Scale bar, 5 μm.

(**B**) Quantification of CTL shape (roundness coefficient) in unconjugated and conjugated CTLs. A circular shape corresponds to an index of 1. Each dot represents one CTL. Bars represent mean values.

(**C**) Representative time-lapse images showing examples of CTL-tumor conjugates resulting in either no detectable response, transient calcium response or sustained calcium response in the target cell. Arrows show actin accumulation at the immunological synapse. Scale bar, 5 μm.

(**D**) Quantification of CTL roundness for contacts in the three indicated categories. Each dot represents one CTL. Red bars represent mean values.

(**E**) Quantification of actin accumulation at the immunological synapse for CTLs engaged in contacts with the indicated outcome. Each dot represents one CTL. Red bars represent mean values.

Data information: Data were pooled from three independent experiments. (***$p<0.001$, ns, not significant, unpaired t-test).

Figure 4: Delivery of sublethal hits dominates CTL activity *in vivo*

Mice with established B cell lymphoma expressing the Twitch-2B calcium indicator were adoptively transferred with GFP-expressing OT-I CTLs. Intravital imaging of the bone marrow was performed on day 2 post T cell transfer.

(**A**) Representative time-lapse images showing tumors without CTLs (upper panels) or with OT-I CTLs (lower panels). Tumor cells with low and high intracellular calcium appear in blue and red, respectively. CTLs appear in white. Red arrows indicate tumor cells with elevated calcium. Scale bar, 5 μm.

(**B**) Calcium responses in individual tumors cells were recorded in (upper table) control tumors (developing without T cells) or (lower table) after T cell transfer in tumor cells contacted by at least one CTL during the imaging period. Data is representative of three independent experiment.

(**C**) Calcium responses of a representative tumor cell in control tumors (blue) or of a tumor cell contacted by a CTL in adoptively transferred mice (red).

(**D**) Quantification of the number of distinct calcium fluxes normalized to 100 min in individual tumor cells. Each dot represents one tumor cell. Red bars represent mean values.

(**E**) Quantification of the cumulated period of calcium signals in individual tumor cells expressed as the percentage of total time. Each dot represents one tumor cell. Bars represent mean values.

(**F**) Pie chart showing the outcomes of CTL-tumor contacts. Contacts were classified into 3 categories: no calcium elevation in the target (no hit), transient calcium elevation (sublethal hit), prolonged calcium response in the target (putative lethal hit).

Data information: Data were pooled of four independent experiments. (*$p<0.05$, ***$p<0.001$, unpaired t-test).

Figure 5: Extensive functional heterogeneity within tumor-infiltrating CTLs *in vivo*

(**A-B**) CTLs exhibit distinct capacities to trigger calcium responses in contacted tumor cells. Mice with established B cell lymphoma expressing OVA and the Twitch-2B calcium indicator were adoptively transferred with GFP-expressing OT-I CTLs. Intravital imaging of the bone marrow was performed two days after T cell transfer. (**A**) *Left*. Two-photon time-lapse image and corresponding scheme showing representative CTLs triggering either limited (upper images) or numerous (lower images) calcium signals in 5 contacted targets. Red arrows mark tumor cells with elevated calcium. Scale bar, 5 µm. *Right*. The periods of contact for the indicated targets are shown as white boxes and periods of calcium elevation are shown in magenta. (**B**) Total number of distinct calcium fluxes triggered by individual CTLs in all contacted tumor cells during an imaging period of one hour. For a rigorous comparison, only CTLs which activity could be monitored for at least 1 h were included in the analysis. Data are representative of 4 independent experiments.

(**C-E**) CTLs exhibit extensive differences in lytic activity *in vivo*. Mice with established B cell lymphoma expressing OVA and the caspase 3 reporter were adoptively transferred with LifeAct-GFP-expressing OT-I CTLs. Intravital imaging of the bone marrow was performed two days after T cell transfer. The frequency of CTLs engaged in lytic activity (induction of apoptosis in at least one contacted tumor cell) is shown (**C**) together with the frequency of lytic contacts within all CTL-tumor cell contacts recorded (**D**). (**E**) Representative two-photon time-lapse images showing a representative CTL with high lytic capacity (killing 4 targets) and a CTL with no lytic activity for up to 4 hours. Blue arrows mark apoptotic tumor cells. Live and apoptotic tumors appear in grey and blue, respectively. CTLs appear in green. Scale bar, 10 µm. Representative of 3 independent experiments.

Figure 6: A minority of CAR T cell-tumors interactions results in target cell apoptosis *in vitro*

Eμ-myc B cells expressing a FRET-based reporter for caspase 3 activity were labeled with the calcium-sensitive dye Indo-1, incubated with GFP-expressing anti-CD19 CAR T cells and subjected to live imaging.

(**A-B**) Calcium responses were recorded over time in (**A**) unconjugated tumor cells or in (**B**) tumor cells forming a conjugate with a CAR T cell. Each line corresponds to an individual tumor cell and each square to a time point. Squares are colored in magenta upon calcium elevation or in blue otherwise. Apoptotic events (detected by caspase 3 activity) are indicated by an overlaid green dot. Data is representative of three independent experiment.

(**C**) The number of calcium fluxes in individual tumor cells is plotted for unconjugated tumors or conjugated tumors. Values were normalized to 100 min. Each dot represents one tumor cell. Bars represent mean values. **p<0.01, unpaired t-test.

(**D**) The cumulated period of calcium signals was recorded for individual unconjugated or conjugated target cells and expressed as percentage of total time. Each dot represents one tumor cell. Bars represent mean values. **p<0.01, unpaired t-test.

(**E**) Distinct tumor cell outcomes in response to CAR T cell attack. Three categories were defined as previously described: no hit, sublethal hit, lethal hit. Pie chart representing the percentage of each category. Data were pooled from three independent experiments with 3 distinct image acquisitions in each experiment.

Figure 7: Heterogeneity in CAR T cell-tumor cells outcome *in vivo*

Mice with established B cell lymphoma expressing the Twitch-2B calcium indicator were adoptively transferred with GFP-expressing anti-CD19 CAR T cells. Intravital imaging of the bone marrow was performed on day 2 post CAR T cell transfer.

(**A**) Representative time-lapse images showing tumors without CAR T cells (upper panels) or with CAR T Cells (lower panels). Tumor cells with low and high intracellular calcium appear

in blue and red, respectively. CAR T cells appear in light green. Red arrows indicate tumor cells with elevated calcium. Scale bar, 5 μm.

(**B**) Calcium responses in individual tumors cells were recorded in (upper table) control tumors (developing without CAR T cells) or (lower table) after CAR T cell transfer in tumor cells contacted by at least one CAR T cell during the imaging period. Representative of 3 independent experiments. Data is representative of three independent experiment.

(**C**) Quantification of the number of distinct calcium fluxes normalized to 100 min in individual tumor cells. Each dot represents one tumor cell. Red bars represent mean values. *$p<0.05$, unpaired t-test.

(**D**) Quantification of the cumulated period of calcium signals in individual tumor cells expressed as the percentage of total time. Each dot represents one tumor cell. Bars represent mean values. ***$p<0.001$, unpaired t-test.

(**E**) Pie chart showing the outcomes of CAR T cell-tumor contacts. Contacts were classified into 3 categories: no calcium elevation in the target (no hit), transient calcium elevation (sublethal hit), prolonged calcium response in the target (putative lethal hit). Data were pooled from three independent experiments.

(**F-G**) CAR T cells exhibit distinct capacities to trigger calcium responses in contacted tumor cells. (**F**) Left. Two-photon time-lapse image and corresponding scheme showing representative CAR T cell triggering either limited (upper images) or numerous (lower images) calcium signals in 4 contacted targets. Red arrows mark tumor cells with elevated calcium. Scale bar, 10 μm. Right. The periods of contact for the indicated targets are shown as white boxes and periods of calcium elevation are shown in magenta. (**G**) Total number of distinct calcium fluxes triggered by individual CAR T cells in all contacted tumor cells during an imaging period of one hour is plotted. For a rigorous comparison, only CAR T cells which

activity could be monitored for at least 1 h were included in the analysis. Data are representative of three independent experiments.

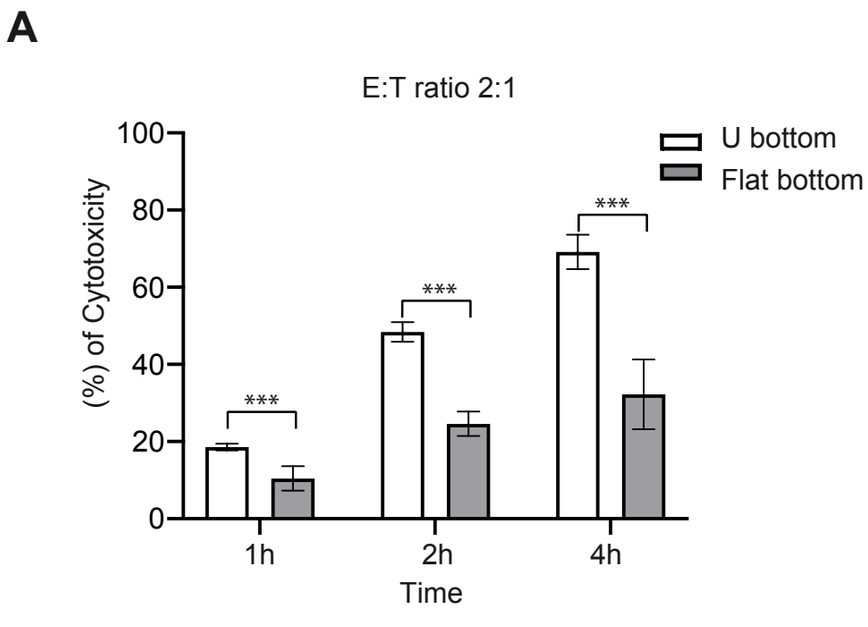
A
E:T ratio 2:1
U bottom
Flat bottom
(%) of Cytotoxicity
100
80
60
40
20
0
***
***
***
1h
2h
4h
Time

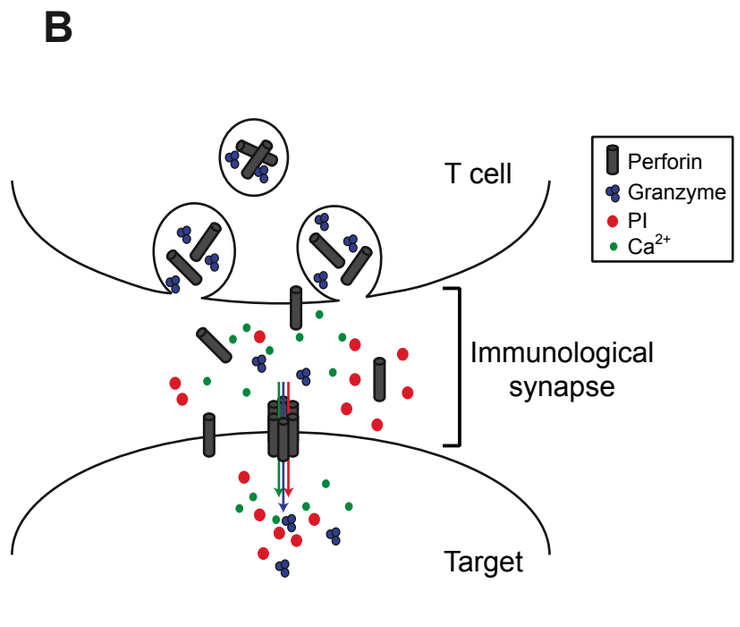
B
T cell
Perforin
Granzyme
PI
Ca2+
Immunological synapse
Target

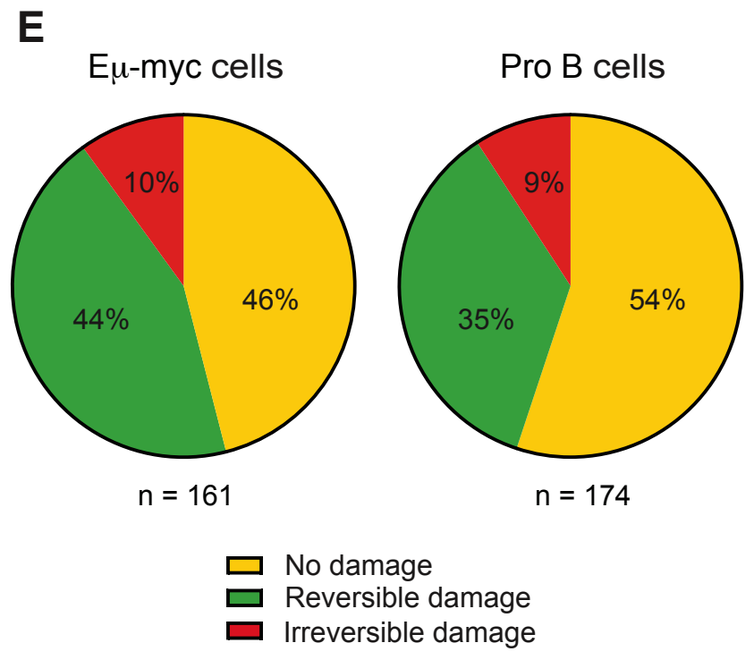
E
Eμ-myc cells
Pro B cells
10%
46%
44%
9%
54%
35%
n = 161
n = 174
No damage
Reversible damage
Irreversible damage

C
No detectable damage
Reversible damage
Irreversible damage
T cells
low Ca2+ high Ca2+
Propidium iodide
0.5 min
2 min
30 min
2min
8 min
30 min
3 min
29 min
38 min

D
T cells
Tumor cells
Calcium
PI
Calcium index
PI uptake
contact
Time (min)

Figure 1

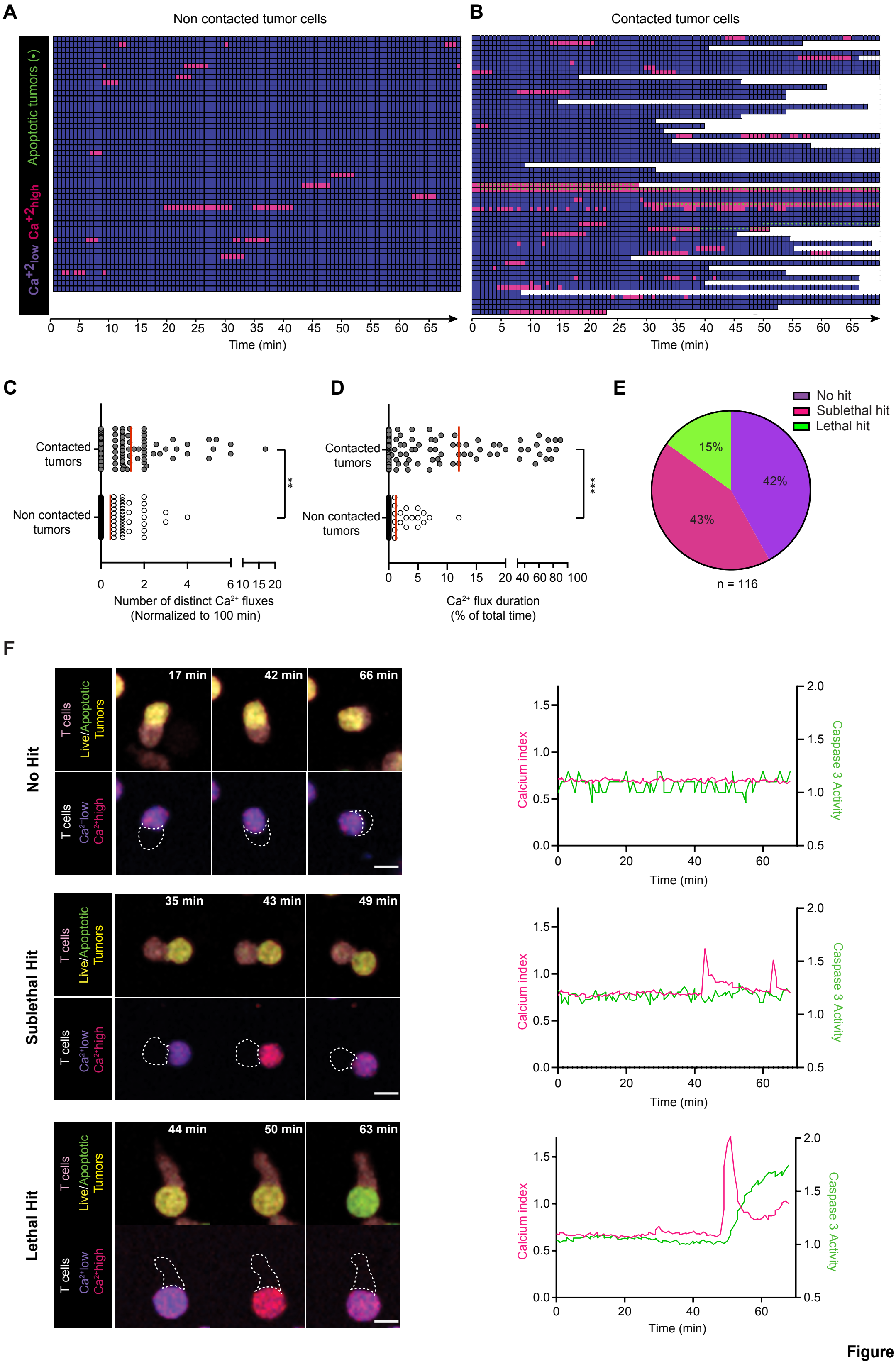
A
Non contacted tumor cells
Apoptotic tumors (•)
Ca+2high
Ca+2low
0 5 10 15 20 25 30 35 40 45 50 55 60 65
Time (min)
B
Contacted tumor cells
0 5 10 15 20 25 30 35 40 45 50 55 60 65
Time (min)
C
Contacted tumors
Non contacted tumors
**
0 2 4 6 10 15 20
Number of distinct Ca2+ fluxes
(Normalized to 100 min)
D
Contacted tumors
Non contacted tumors
***
0 5 10 15 20 40 60 80 100
Ca2+ flux duration
(% of total time)
E
No hit
Sublethal hit
Lethal hit
15%
42%
43%
n = 116
F
No Hit
Sublethal Hit
Lethal Hit
T cells
Live/Apoptotic Tumors
T cells
Ca2+low
Ca2+high
17 min
42 min
66 min
35 min
43 min
49 min
44 min
50 min
63 min
Calcium index
Caspase 3 Activity
0.0 0.5 1.0 1.5
0.5 1.0 1.5 2.0
0 20 40 60
Time (min)

Figure 2

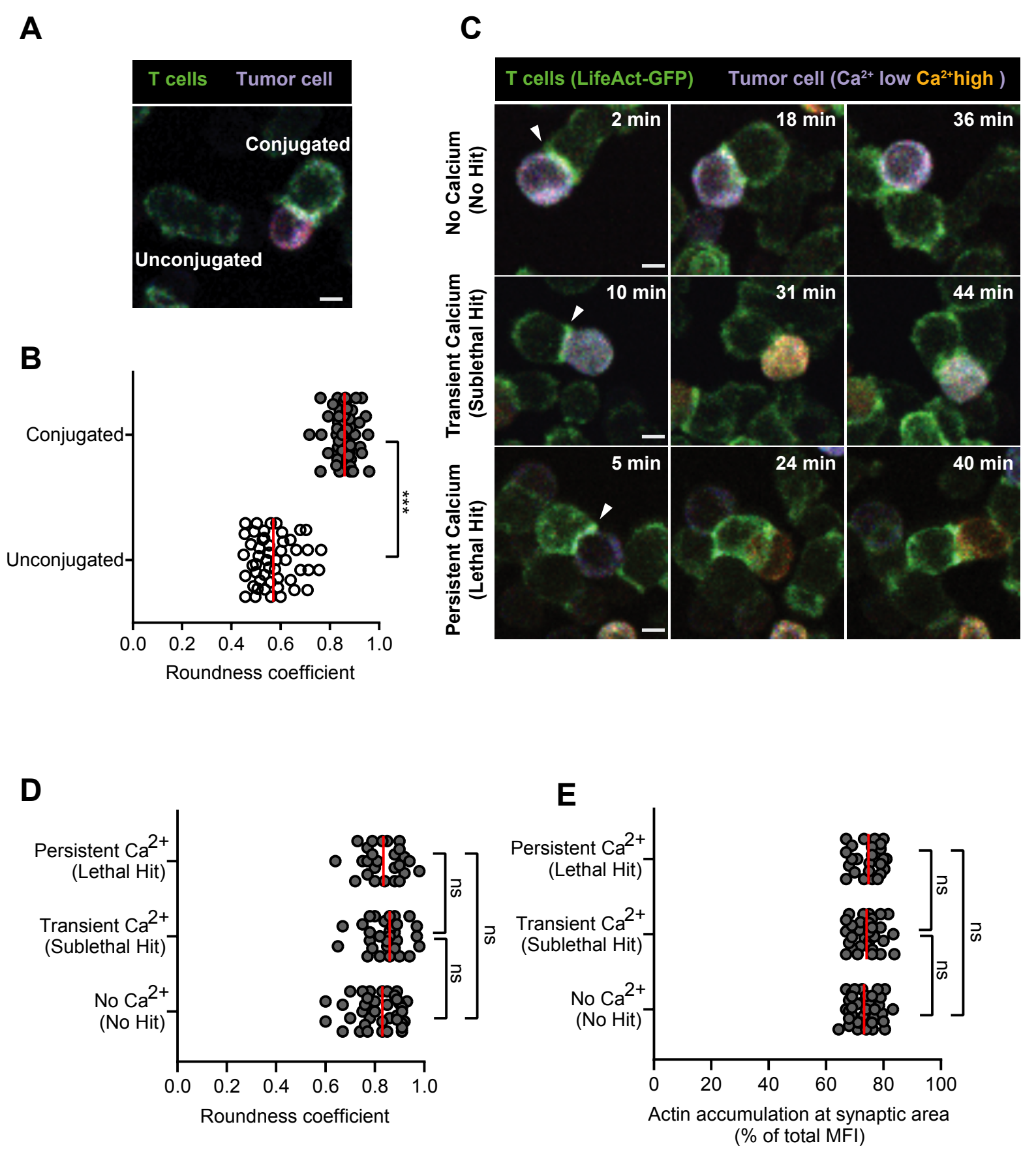
A
T cells
Tumor cell
Conjugated
Unconjugated
B
Conjugated
Unconjugated
***
0.0
0.2
0.4
0.6
0.8
1.0
Roundness coefficient
C
T cells (LifeAct-GFP)
Tumor cell (Ca2+ low Ca2+high)
No Calcium (No Hit)
Transient Calcium (Sublethal Hit)
Persistent Calcium (Lethal Hit)
2 min
18 min
36 min
10 min
31 min
44 min
5 min
24 min
40 min
D
Persistent Ca2+ (Lethal Hit)
Transient Ca2+ (Sublethal Hit)
No Ca2+ (No Hit)
ns
ns
ns
0.0
0.2
0.4
0.6
0.8
1.0
Roundness coefficient
E
Persistent Ca2+ (Lethal Hit)
Transient Ca2+ (Sublethal Hit)
No Ca2+ (No Hit)
ns
ns
ns
0
20
40
60
80
100
Actin accumulation at synaptic area (% of total MFI)

Figure 3

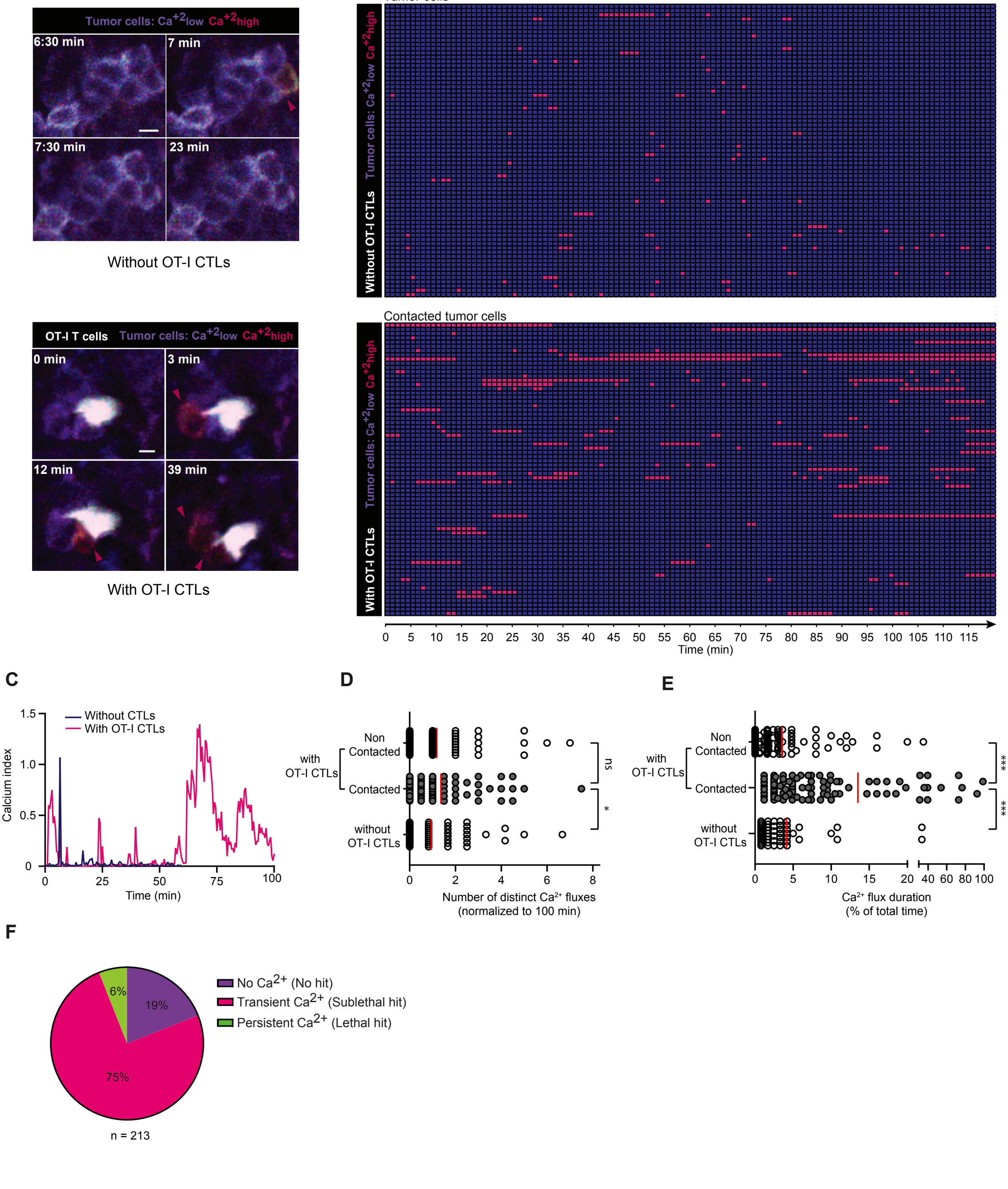
A
Tumor cells: Ca+2low Ca+2high
6:30 min
7 min
7:30 min
23 min
Without OT-I CTLs
OT-I T cells
Tumor cells: Ca+2low Ca+2high
0 min
3 min
12 min
39 min
With OT-I CTLs
B
Tumor cells
Without OT-I CTLs
Tumor cells: Ca+2low Ca+2high
Contacted tumor cells
With OT-I CTLs
Tumor cells: Ca+2low Ca+2high
0 5 10 15 20 25 30 35 40 45 50 55 60 65 70 75 80 85 90 95 100 105 110 115
Time (min)
C
Without CTLs
With OT-I CTLs
Calcium index
1.5
1.0
0.5
0
0 25 50 75 100
Time (min)
D
Non Contacted
with OT-I CTLs
Contacted
without OT-I CTLs
ns
*
0 2 4 6 8
Number of distinct Ca2+ fluxes
(normalized to 100 min)
E
Non Contacted
with OT-I CTLs
Contacted
without OT-I CTLs
***
***
0 5 10 15 20 40 60 80 100
Ca2+ flux duration
(% of total time)
F
6%
19%
75%
No Ca2+ (No hit)
Transient Ca2+ (Sublethal hit)
Persistent Ca2+ (Lethal hit)
n = 213

Figure 4

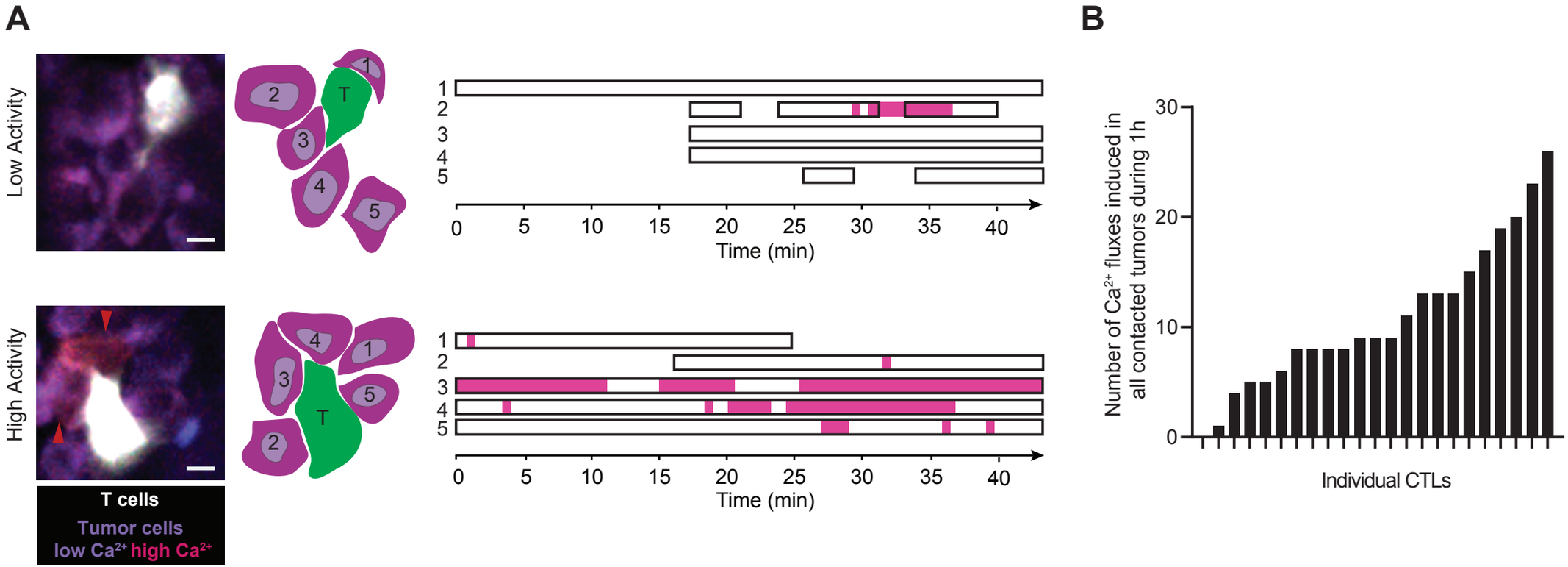
A
Low Activity
High Activity
T cells
Tumor cells
low Ca2+ high Ca2+
Time (min)
B
Number of Ca2+ fluxes induced in all contacted tumors during 1h
Individual CTLs
C
Lytic CTLs
Non lytic CTLs
20%
80%
n=30
D
Lytic contacts
Unproductive contacts
5%
95%
n=124
E
T cells (LifeAct-GFP)
Target cells Live / Apoptotic
Super killer
Non lytic CTL
0min
19min
53min
2 min
96 min
240 min

Figure 5

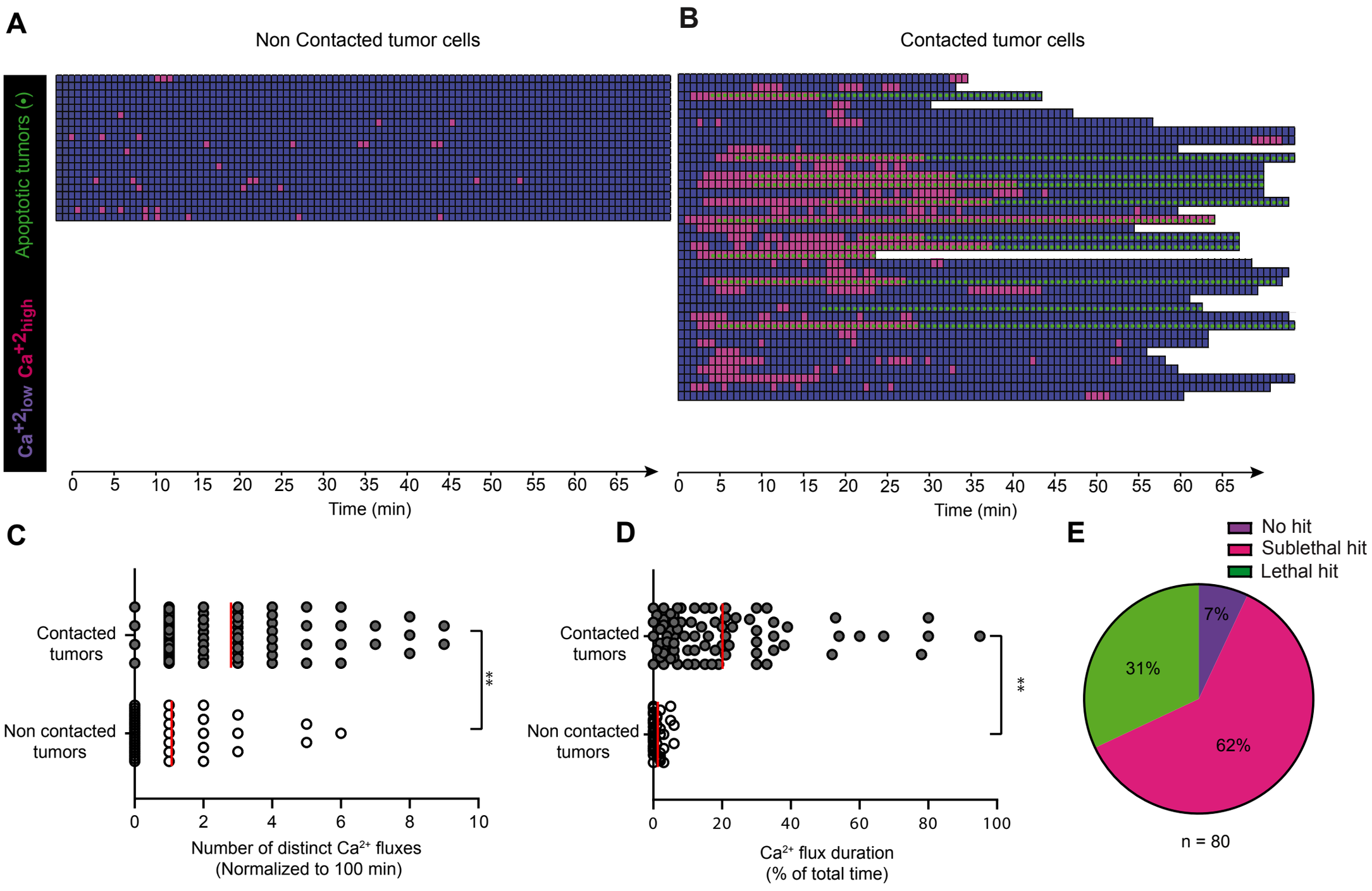
A
Non Contacted tumor cells
B
Contacted tumor cells
Apoptotic tumors (•)
Ca+2low Ca+2high
0 5 10 15 20 25 30 35 40 45 50 55 60 65
Time (min)
C
Contacted tumors
Non contacted tumors
**
0 2 4 6 8 10
Number of distinct Ca2+ fluxes
(Normalized to 100 min)
D
Contacted tumors
Non contacted tumors
**
0 20 40 60 80 100
Ca2+ flux duration
(% of total time)
E
No hit
Sublethal hit
Lethal hit
7%
31%
62%
n = 80

Figure 6

A

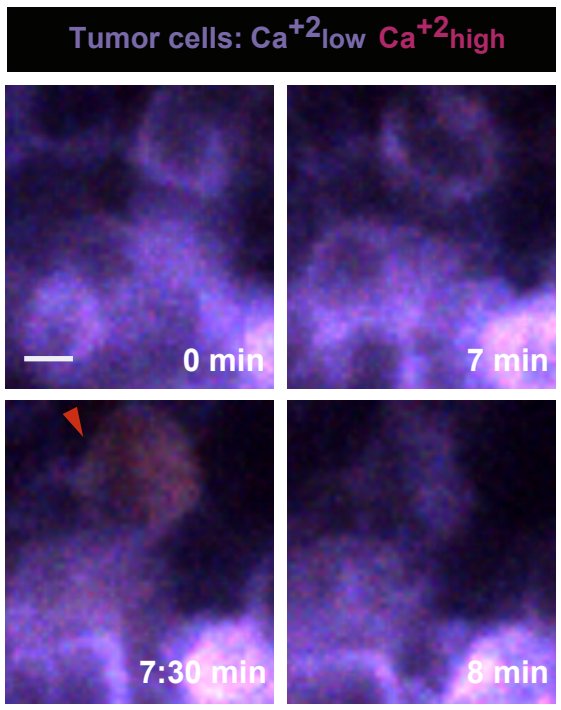

B

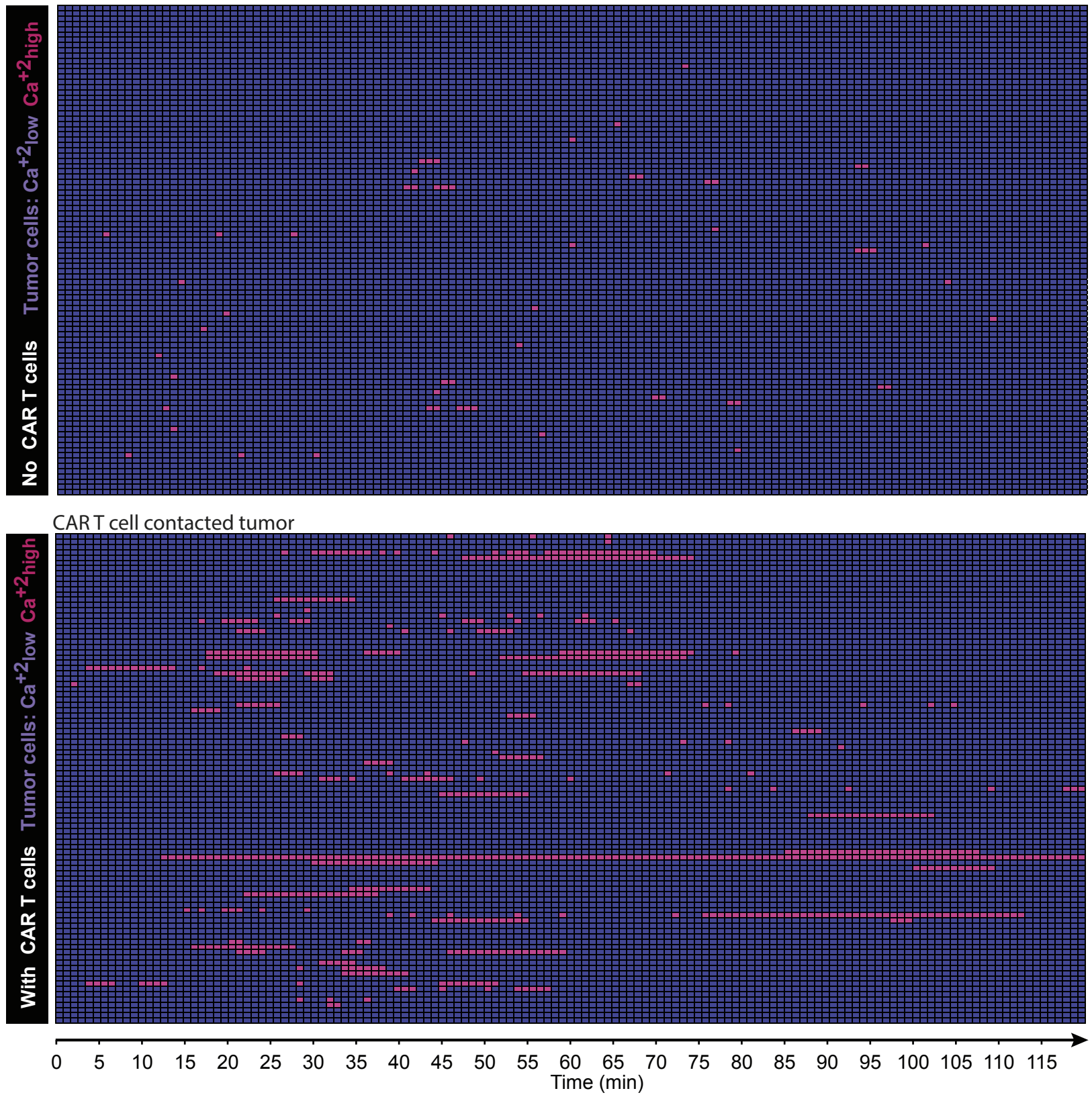

C

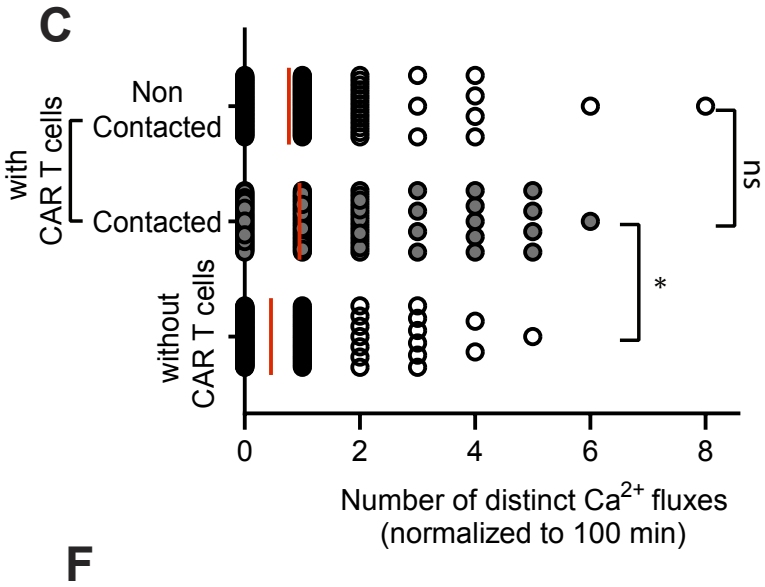

D

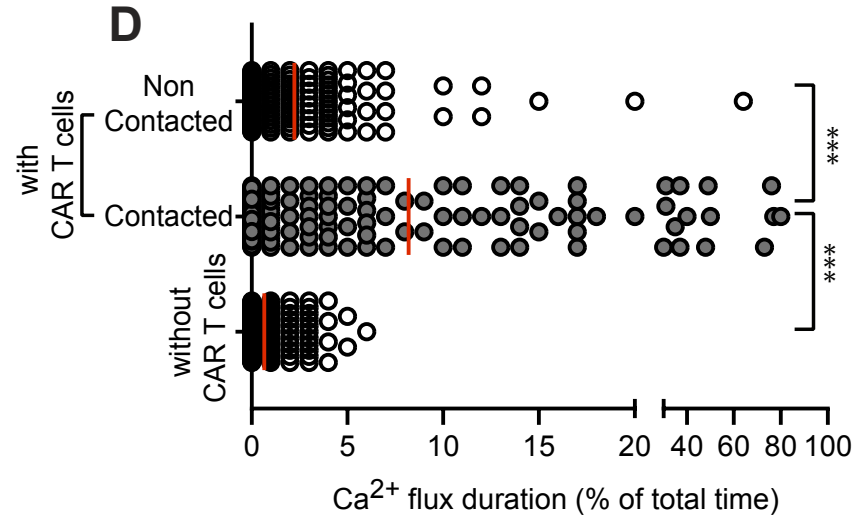

E

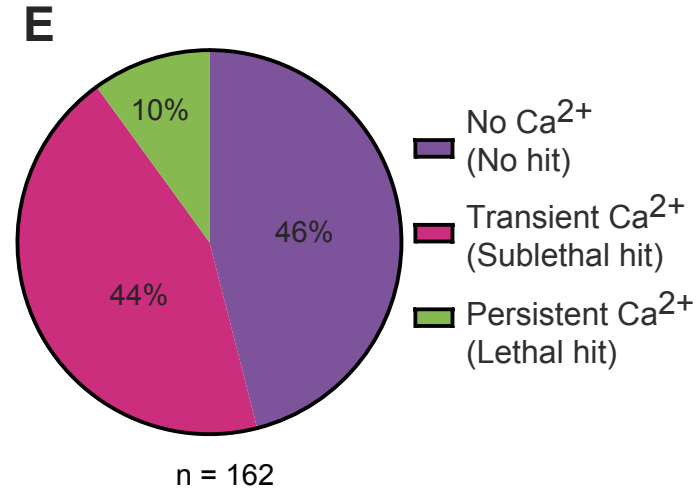

F

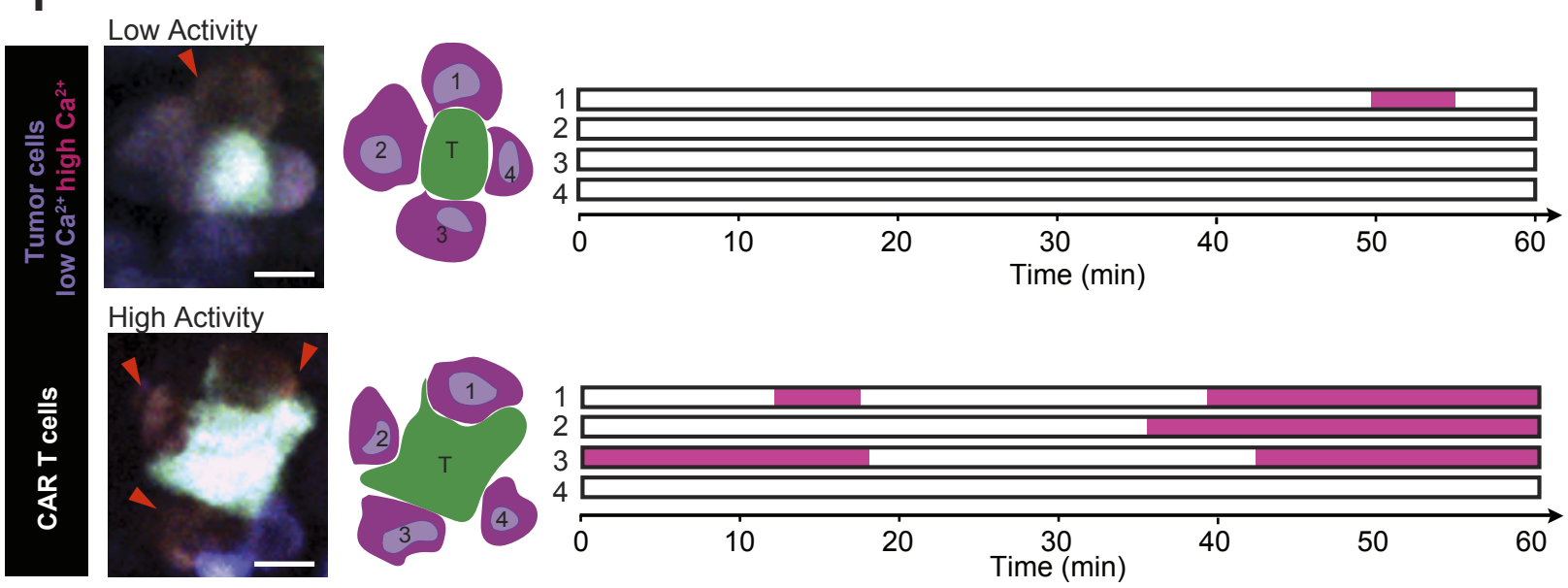

G

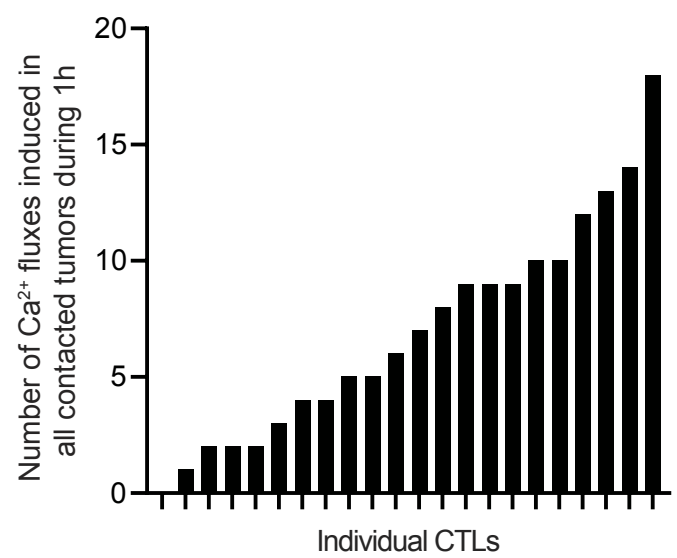

Figure 7